

Contribution of remote bands to orbital magnetization in twisted bilayer graphene

Pinzhuo Li,^{1,2} Kun Jiang,^{3,4} Ziqiang Wang,^{5,*} Jian Kang,^{1,†} and Yi Zhang^{6,7,‡}

¹*School of Physical Science and Technology, ShanghaiTech University, Shanghai 201210, China*

²*State Key Laboratory of Quantum Functional Materials,*

School of Physical Science and Technology, ShanghaiTech University, Shanghai 201210, China

³*Beijing National Laboratory for Condensed Matter Physics and Institute of Physics, Chinese Academy of Sciences, Beijing 100190, China*

⁴*University of Chinese Academy of Sciences, Beijing 100190, China*

⁵*Department of Physics, Boston College, Chestnut Hill, MA 02467, USA*

⁶*Department of Physics and Institute for Quantum Science and Technology, Shanghai University, Shanghai 200444, China*

⁷*Shanghai Key Laboratory of High Temperature Superconductors, Shanghai University, Shanghai 200444, China*

Motivated by recent theoretical and experimental works on orbital magnetization M_{orb} for the interacting system, we develop a gauge-invariant framework to compute M_{orb} for correlated phases of magic-angle twisted bilayer graphene within self-consistent Hartree-Fock approximation. Based on the projector formulation of the theory of orbital magnetization, we evaluate both M_{orb} and the self-rotation contribution m_{SR} directly from the Hartree-Fock Hamiltonian. We demonstrate that, in contrast to topological invariants such as the Chern number, both M_{orb} and m_{SR} obtain substantial contributions from remote bands and thus require careful convergence with respect to the number of included remote bands. Applying this approach to correlated phases at integer fillings, we obtain converged M_{orb} and m_{SR} for time reversal symmetry broken Chern insulating states at $\nu = \pm 3$ and for competing correlated phases at other integer fillings. Our results establish a systematic and controlled approach for evaluating orbital magnetization in correlated moiré systems and clarify the crucial role of remote bands in determining their magnetic response.

I. INTRODUCTION

The recent discovery of the correlated insulating states [1–9] and unconventional superconductivity [3, 9–11] in twisted bilayer graphene (TBG) has stimulated tremendous research efforts in moiré systems. Due to the extreme flatness of the lowest energy bands in TBG near the magic angle [12] and their nontrivial topology [13–18], electronic Coulomb interactions are believed to drive a rich and robust set of strongly correlated and topological phases. Theoretical studies have predicted several strongly correlated and topologically distinct states at integer fillings [19–42]. Among these states, the time-reversal symmetry breaking (TRSB) phases can become Chern insulators, exhibiting the quantum anomalous Hall (QAH) effect, which have been observed experimentally [2, 8, 43–47]. The ferromagnetic QAH states at $\nu = 3$ filling was discovered to show strong magnetic response to external DC currents [2, 8], which can be understood from the large orbital magnetization of the TBG system as a result of TRSB [48–50]. Specifically, this strong orbital effect has been studied in moiré systems where the time-reversal symmetry is explicitly broken [51, 52], and in the $C_2\mathcal{T}$ symmetric moiré system such as TBG in the presence of additional $C_2\mathcal{T}$ symmetry breaking potential [48, 49].

Moreover, the transport and scanning tunneling microscopy (STM) experiments revealed that weak to moderate out-of-plane magnetic fields can turn the ground states at $\nu = \pm 1, \pm 2, \pm 3$ into strong-correlation induced Chern insulators in magic-angle TBG [44, 45]. The associated orbital magnetization plays a central role in these phenomena, which

determines the coupling to external magnetic fields. Understanding orbital magnetization in correlated moiré systems is therefore essential for elucidating the microscopic origin of Chern insulators and field-induced quantum phase transitions in TBG [44–47].

Theoretically, the Berry curvature and orbital magnetic moments of moiré bands have been extensively analyzed within the non-interacting Bistritzer–MacDonald (BM) continuum model [48, 53–55]. These studies established that the flat bands of TBG can host nontrivial topology and substantial orbital magnetization per unit cell largely arising from sizable Berry curvature. However, the flat-band nature of magic-angle TBG implies that electron–electron interactions are comparable to or even larger than the bandwidth, and self-consistent Hartree–Fock (HF) calculations have demonstrated that interactions tremendously reconstruct the band structure and stabilize correlated Chern insulating states at integer fillings [19–42]. Despite this progress, a systematic calculation of the bulk orbital magnetization in such interaction-driven states remains lacking. In particular, it is not clear how interaction-induced band reconstruction, valley polarization, and remote-band contributions quantitatively modify the orbital magnetization from the non-interacting predictions, nor how these effects relate to experimentally observed field-induced switching between competing correlated phases.

In this work, we adopt the recently-developed method [56–60] and develop a gauge-invariant framework [61] for computing orbital magnetization within self-consistent Hartree–Fock theory and apply it to correlated insulating states of magic-angle TBG. Starting from the BM continuum model with Coulomb interactions projected onto the relevant bands, we determine symmetry-broken ground states at integer fillings and evaluate the orbital magnetization using the modern theory expressed in terms of projection operators. This formulation avoids gauge ambiguities and enables a controlled treat-

* ziqiang.wang@bc.edu

† kangjian@shanghaitech.edu.cn

‡ zhangyi821@shu.edu.cn

ment of the large number of remote bands inherent to the continuum description. We demonstrate that, unlike topological invariants such as the Chern number, the orbital magnetization exhibits a pronounced sensitivity to remote-band contributions and requires careful convergence. Applying this framework, we compute both the total orbital magnetization M_{orb} and the self-rotation (local circulation) component m_{SR} relevant for magneto-optical measurements such as magnetic circular dichroism (MCD). The calculated orbital magnetization respects the particle-hole symmetry that relates the fillings of ν and $-\nu$ [35] and reproduces the characteristic linear dependence of magnetization on chemical potential within the insulating gap, with slope proportional to the Chern number. We further analyze the sign structure of the magnetization and its relation to changes in Hall conductivity. At $\nu = \pm 1$, we compare competing Chern and intervalley-coherent states and show that Chern insulating phases possess substantially larger orbital magnetization, providing a microscopic explanation for their stabilization under external magnetic fields. Our results establish a systematic approach for evaluating orbital magnetization in correlated moiré systems and elucidate the important role of interactions as well as the critical contribution of remote bands in shaping orbital ferromagnetism in twisted bilayer graphene.

II. NON-INTERACTING MODEL

The moiré pattern in TBG is formed by twisting the top and bottom layers of an aligned bilayer graphene by angles $\theta/2$ and $-\theta/2$, which forms a periodic superlattice structure of a triangular lattice with the lattice vectors $\mathbf{L}_{M1} = (0, -1)L_M$, $\mathbf{L}_{M2} = (\frac{\sqrt{3}}{2}, -\frac{1}{2})L_M$ and $L_M = a_0/(2 \sin(\theta/2))$, where $a_0=0.246$ nm, is the lattice constant of the monolayer graphene. The corresponding reciprocal lattice vectors of the moiré lattice are $\mathbf{G}_1 = (-\frac{2\pi}{\sqrt{3}L_M}, -\frac{2\pi}{L_M})$ and $\mathbf{G}_2 = (\frac{4\pi}{\sqrt{3}L_M}, 0)$. The non-interacting physics of TBG can be described by the continuum model introduced by Bistritzer and MacDonald [12, 62]. The Hamiltonian of the continuum model for each valley is given by,

$$H_{BM}^\tau(\hat{\mathbf{k}}) = \begin{pmatrix} -\hbar v_F(\hat{\mathbf{k}} - \mathbf{K}_1^\tau) \cdot \boldsymbol{\sigma}^\tau & U \\ U^\dagger & -\hbar v_F(\hat{\mathbf{k}} - \mathbf{K}_2^\tau) \cdot \boldsymbol{\sigma}^\tau \end{pmatrix} \quad (1)$$

where $\hat{\mathbf{k}} = -i\partial_{\mathbf{r}}$, $\tau = \pm$ is the valley index, and $\boldsymbol{\sigma}^\tau = (\tau\sigma_x, \sigma_y)$ the Pauli matrices acting in the A,B sublattice space. In Eq. (1), \mathbf{K}_1^τ and \mathbf{K}_2^τ are the Dirac points of valley τ in the bottom and top layers that are twisted by angles $\mp\frac{\theta}{2}$, which are equivalent to $-\tau\mathbf{K}_1$ and $-\tau\mathbf{K}_2$ in the mBZ as shown in Fig. 1(c). The interlayer tunneling between the Dirac states in the two layers is described by the matrix

$$U = \begin{pmatrix} u_0 & u_1 \\ u_1 & u_0 \end{pmatrix} + \begin{pmatrix} u_0 & u_1 e^{-i\tau\frac{2\pi}{3}} \\ u_1 e^{i\tau\frac{2\pi}{3}} & u_0 \end{pmatrix} e^{-i\tau\mathbf{G}_1 \cdot \mathbf{r}} + \begin{pmatrix} u_0 & u_1 e^{i\tau\frac{2\pi}{3}} \\ u_1 e^{-i\tau\frac{2\pi}{3}} & u_0 \end{pmatrix} e^{-i\tau(\mathbf{G}_1 + \mathbf{G}_2) \cdot \mathbf{r}} \quad (2)$$

where u_0 and u_1 are the intra- and inter-sublattice interlayer tunneling amplitudes. We adopt realistic parameters for the

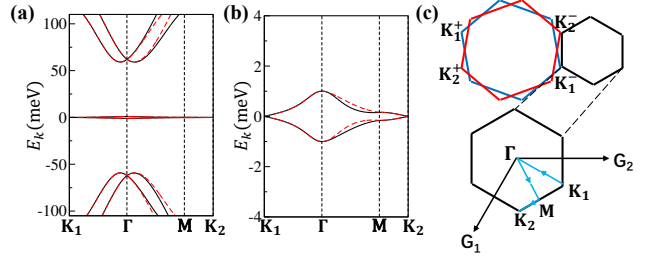


FIG. 1. (a) Low-energy band structure of non-interacting TBG calculated using the BM model. The black solid and red dashed curves correspond to the K' and K valleys, respectively. (b) Zoomed-in view of the isolated flat bands near charge neutrality, highlighting their separation from the higher-energy remote bands. (c) Schematic illustration of Brillouin zone folding in TBG. The small hexagon denotes the moiré Brillouin zone (mBZ), reciprocal to the moiré superlattice. The cyan arrows indicate the momentum path in the enlarged moiré Brillouin zone along which the band dispersions in panels (a) and (b) are plotted.

continuum model: $\hbar v_F/a_0 = 2.365$ eV, inter-sublattice interlayer coupling $u_1 = 0.11$ eV, and intra-sublattice interlayer coupling $u_0 = 0.06$ eV. The twist angle is fixed at the magic value $\theta=1.086^\circ$, at which the low-energy moiré bands become perfectly flat in the limit $u_0 \rightarrow 0$ [16]. The low-energy flat bands exhibit a bandwidth of approximately 2 meV and are well separated from the higher-energy remote bands by an energy gap of about 50 meV as shown in Fig. 1. The eigenstates of the continuum Hamiltonian H_{BM}^τ have the Bloch wavefunction form

$$\psi_{m,\tau,\mathbf{k}}^X(\mathbf{r}) = \sum_{\mathbf{G}} u_{m,\tau,\mathbf{G},X}(\mathbf{k}) e^{i(\mathbf{k}+\mathbf{G}) \cdot \mathbf{r}} \quad (3)$$

where $X = \{A_1, B_1, A_2, B_2\}$ is the layer and sublattice index with the eigen-band energy $\epsilon_{m\mathbf{k}\tau}$ and \mathbf{G} is the general reciprocal lattice vector in the mBZ. Here, m and τ are the band and valley indices, and the spin index s is omitted since the Hamiltonian is spin independent.

III. INTERACTING CASE

The full Hamiltonian $H = H_0 + H_{int}$ contains the non-interacting part

$$H_0 = \sum_{\tau} H_{BM}^\tau = \sum_{m\mathbf{k}\tau} \epsilon_{m\mathbf{k}\tau} d_{m\mathbf{k}\tau}^\dagger d_{m\mathbf{k}\tau}, \quad (4)$$

where $d_{m\mathbf{k}\tau}^\dagger$ and $d_{m\mathbf{k}\tau}$ are the creation and annihilation operators in the eigen-band basis. To incorporate interactions, we project the Coulomb interaction onto the two lowest-energy flat bands per spin and per valley, and perform self-consistent Hartree-Fock calculations directly in momentum space. This approach avoids the real-space Wannier obstruction associated with topological flat bands [14, 15, 18, 63, 64]. Further technical details of the Hartree-Fock procedure can be found in the Appendix of Ref.22. The interacting part of the Hamil-

tonian is written as[35, 65]

$$H_{int} = \frac{1}{2S} \sum_{\mathbf{q} \neq 0} V(\mathbf{q}) \delta \rho_{\mathbf{q}} \delta \rho_{-\mathbf{q}}, \quad (5)$$

where S is the total area and $\delta \rho_{\mathbf{q}} = \rho_{\mathbf{q}} - \bar{\rho}_{\mathbf{q}}$ is the density operator relative to charge neutrality of the decoupled bilayer graphene in momentum space. We note that this interaction form is somewhat different from the normal ordered interactions supplemented by double-counting subtraction schemes used in previous Hartree-Fock (HF) studies [22, 28, 30]. It is believed that the Coulomb interaction expressed in Eq. 5 has the advantage of partially accounting for the renormalization and screening effects of the remote bands on the lowest flat bands [35, 65]. The density operator can be expanded in the eigen-basis of H_0 ,

$$\rho_{\mathbf{q}} = \sum_{s,\tau} \sum_{\mathbf{k} \in \text{mBZ}, m_1, m_2} \lambda_{m_1, m_2; \tau}(\mathbf{k}, \mathbf{k} + \mathbf{q}) d_{\mathbf{k}, m_1, s, \tau}^\dagger d_{\mathbf{k} + \mathbf{q}, m_2, s, \tau} \quad (6)$$

with the quantum averaged background density

$$\bar{\rho}_{\mathbf{q}} = \sum_{\mathbf{G}, \tau, m} \delta_{\mathbf{q}, \mathbf{G}} \sum_{\mathbf{k} \in \text{mBZ}} \lambda_{m, m; \tau}(\mathbf{k}, \mathbf{k} + \mathbf{G}), \quad (7)$$

where λ is the form factor defined in terms of the Bloch wave-function as

$$\begin{aligned} \lambda_{m_1, m_2; \tau}(\mathbf{k}, \mathbf{k} + \mathbf{q}) &= \langle u_{m_1, \tau}(\mathbf{k}) | u_{m_2, \tau}(\mathbf{k} + \mathbf{q}) \rangle \\ &= \sum_{\mathbf{G}', X} u_{m_1, \tau; \mathbf{G}', X}^*(\mathbf{k}) u_{m_2, \tau; \mathbf{G}', X}(\mathbf{k} + \mathbf{q}). \end{aligned} \quad (8)$$

Here, \mathbf{k} is restricted in the mBZ while \mathbf{q} can extend to the original Brillouin zone of the monolayer graphene. The operator d^\dagger obeys the periodic condition $d_{m\mathbf{k}s\tau}^\dagger = d_{m\mathbf{k}+\mathbf{G}s\tau}^\dagger$, which is equivalent to the Bloch wave function obeying the condition $u_{m,\tau;\mathbf{G},X}(\mathbf{k} + \mathbf{G}_0) = u_{m,\tau;\mathbf{G}+\mathbf{G}_0,X}(\mathbf{k})$. We take $V(\mathbf{q})$ as the single-gate-screened Coulomb potential [30]

$$V(\mathbf{q}) = \frac{e^2}{2\epsilon\epsilon_0 q} (1 - e^{-2qd_s}) \quad (9)$$

In this paper, we take the dielectric constant $\epsilon = 7$ and the gate distance $d_s = 40$ nm.

It is well established that electron–electron Coulomb interactions in twisted bilayer graphene can drive spontaneous symmetry breaking, giving rise to a series of correlated insulating states at commensurate integer fillings. Among these, states that break the combined $C_2\mathcal{T}$ symmetry are energetically competitive. In particular, at fillings $\nu = \pm 3$, the $C_2\mathcal{T}$ -broken Chern insulating states can emerge as ground states even in the absence of an explicit staggered sublattice potential. In this work, we systematically identify the correlated insulating states at all integer fillings within the Hartree–Fock approximation and compute the orbital magnetization of these interaction-driven phases.

IV. ORBITAL MAGNETIZATION

The topology of the correlated electronic states and their response to an external magnetic field are governed by the Berry curvature and orbital magnetization of the interaction-renormalized bands. In our approach, the Coulomb interaction is projected onto the lowest two flat bands per spin and per valley. As a consequence, only those HF renormalized flat bands that break the combined $C_2\mathcal{T}$ symmetry can acquire nontrivial Berry curvature and hence finite Chern numbers. Since the Berry curvature depends only on the periodic part of the Bloch wave functions, it can be directly computed from the HF eigenstates as

$$\Omega_n(\mathbf{k}) = i \sum_{\mu\nu} \epsilon_{\mu\nu} \langle \partial_\mu u_n^{HF}(\mathbf{k}) | \partial_\nu u_n^{HF}(\mathbf{k}) \rangle, \quad (10)$$

where n denotes the band index, $\epsilon_{\mu\nu}$ is the antisymmetric tensor, μ, ν are Cartesian indices, and $\partial_\mu \equiv \partial/\partial k_\mu$. For the orbital magnetization, it has been recently shown [56] that both the total orbital magnetization M_{orb} and the self-rotation contribution m_{SR} can be evaluated using the HF Hamiltonian and its eigenfunctions [66–68]:

$$M_{\text{orb}} = \frac{e}{2i\hbar} \sum_{n\mathbf{k}} \sum_{\mu\nu} \epsilon_{\mu\nu} \langle \partial_\mu u_n(\mathbf{k}) | (H^{HF}(\mathbf{k}) + \epsilon_n^{HF}(\mathbf{k}) - 2\mu) | \partial_\nu u_n(\mathbf{k}) \rangle n_F(\epsilon_n^{HF}(\mathbf{k}) - \mu) \quad (11)$$

$$m_{\text{SR}} = \frac{e}{2i\hbar} \sum_{n,\alpha} \sum_{\mathbf{k}} \sum_{\mu\nu} \epsilon_{\mu\nu} \langle \partial_\mu u_n(\mathbf{k}) | u_\alpha(\mathbf{k}) \rangle (\epsilon_\alpha^{HF}(\mathbf{k}) - \epsilon_n^{HF}(\mathbf{k})) \langle u_\alpha(\mathbf{k}) | \partial_\nu u_n(\mathbf{k}) \rangle n_F(\epsilon_n^{HF}(\mathbf{k}) - \mu) (1 - n_F(\epsilon_\alpha^{HF}(\mathbf{k}) - \mu)) \quad (12)$$

where $n_F(E) = \Theta(\mu - E)$ is the Fermi–Dirac distribution function at $T = 0$ and μ is the chemical potential. These quantities can be reformulated in terms of projection operators.

We emphasize that the Hartree-Fock Hamiltonian $H^{HF}(\mathbf{k})$ must be formulated in the full Hilbert space, including the flat-band sector as well as both the occupied and empty

remote bands. In principle, Eqs. 11 and 12 involve summations over all occupied states in both the active and remote bands, rendering the calculation formally infinite. To make the numerical calculations tractable, we evaluate M_{orb} and m_{SR} in a truncated Hilbert space. For clarity of notation, we label the HF Bloch states $|u_n^{A/R+/R-}(\mathbf{k})\rangle$ by the superscripts A , $R+$, and

R^- , which denote the active bands, the empty remote bands, and the occupied remote bands, respectively. The empty and occupied remote bands are indexed by n , counted outward from the charge neutrality point, such that the states $|u_n^{R^+}(\mathbf{k})\rangle$ and $|u_n^{R^-}(-\mathbf{k})\rangle$ are related by the particle-hole symmetry [35]. On this basis, we introduce two projection operators onto the truncated occupied and empty states.

$$P_{n_{\text{cut}}}(\mathbf{k}) = \sum_{n \in \text{occupied}} |u_n^A(\mathbf{k})\rangle\langle u_n^A(\mathbf{k})| + \sum_{n \leq n_{\text{cut}}} |u_n^{R^-}(\mathbf{k})\rangle\langle u_n^{R^-}(\mathbf{k})| \quad (13)$$

$$Q_{n_{\text{cut}}}(\mathbf{k}) = \sum_{n \in \text{empty}} |u_n^A(\mathbf{k})\rangle\langle u_n^A(\mathbf{k})| + \sum_{n \leq n_{\text{cut}}} |u_n^{R^+}(\mathbf{k})\rangle\langle u_n^{R^+}(\mathbf{k})|, \quad (14)$$

These two projection operators for truncated occupied and empty states explicitly depend on the choice of n_{cut} , and thus $P_{n_{\text{cut}}}(\mathbf{k}) + Q_{n_{\text{cut}}}(\mathbf{k}) = I$ only when $n_{\text{cut}} \rightarrow \infty$. In this representation, we introduce the orbital magnetization for the truncated Hilbert space that is expressed as [69]

$$M_{\text{orb}}^{\text{trun}} = -\frac{e}{\hbar} \sum_{\mathbf{k}} \text{Im} \left[W_{xy}^{\text{trun}}(\mathbf{k}) - N_{xy}^{\text{trun}}(\mathbf{k}) \right] \quad (15)$$

$$m_{\text{SR}}^{\text{trun}} = \frac{e}{\hbar} \sum_{\mathbf{k}} \text{Im} \left[W_{xy}^{\text{trun}}(\mathbf{k}) + N_{xy}^{\text{trun}}(\mathbf{k}) \right], \quad (16)$$

where

$$W_{\mu\nu}^{\text{trun}}(\mathbf{k}) = \text{Tr} \left[P_{n_{\text{cut}}}(\mathbf{k}) (\partial_{\mu} P_{n_{\text{cut}}}(\mathbf{k})) (\partial_{\nu} Q_{n_{\text{cut}}}(\mathbf{k})) (H^{\text{HF}}(\mathbf{k}) - \mu) \right] \quad (17)$$

and

$$N_{\mu\nu}^{\text{trun}}(\mathbf{k}) = \text{Tr} \left[Q_{n_{\text{cut}}}(\mathbf{k}) (\partial_{\mu} P_{n_{\text{cut}}}(\mathbf{k})) (\partial_{\nu} Q_{n_{\text{cut}}}(\mathbf{k})) (H^{\text{HF}}(\mathbf{k}) - \mu) \right]. \quad (18)$$

Because the projection operators $P_{n_{\text{cut}}}(\mathbf{k})$ and $Q_{n_{\text{cut}}}(\mathbf{k})$ are manifestly gauge invariant, this formulation avoids the gauge ambiguities that typically arise in direct evaluations of orbital magnetization based on Bloch wave functions. Moreover, it circumvents the singularities associated with band degeneracy points. Formally, physical quantities are defined in the limit $n_{\text{cut}} \rightarrow \infty$. Nevertheless, we anticipate rapid convergence with increasing n_{cut} , enabling reliable numerical evaluation within a finite truncated Hilbert space.

A. $\nu = \pm 3$

We first consider the case of fillings $\nu = \pm 3$. The self-consistent Hartree–Fock calculation yields a spin–valley polarized Chern insulating ground state characterized by spontaneous breaking of the combined $C_2\mathcal{T}$ symmetry. The corresponding band dispersions, shown in Fig. 2(a) and (b), indicate that among the eight active bands, a single pair associated with one spin–valley flavor develops a gap due to $C_2\mathcal{T}$ symmetry breaking and acquires a finite Chern number. The remaining three pairs of bands, corresponding to

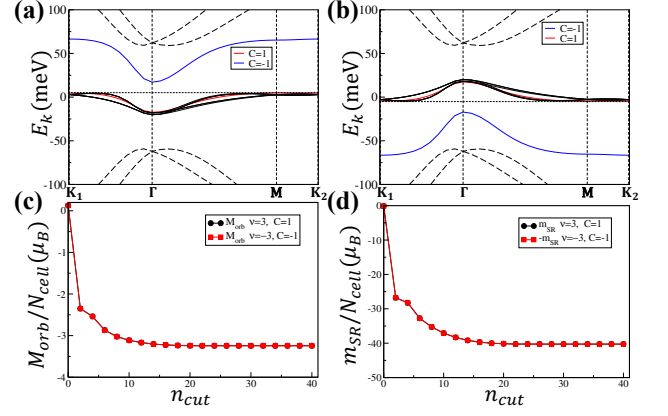


FIG. 2. (a,b) Band dispersions of the Chern insulating states at fillings $\nu = 3$ (a) and $\nu = -3$ (b), obtained within the HF approximation. The solid curves represent the eight interaction-renormalized HF bands, while the dashed curves denote the remote bands that are excluded from the self-consistent HF calculation. Bands carrying nontrivial Chern numbers are highlighted in red ($C = 1$) and blue ($C = -1$), corresponding to the experimentally observed Chern insulating states with $C = \pm 1$ at $\nu = \pm 3$. (c,d) Calculated total orbital magnetization M_{orb} and self-rotation contribution m_{SR} per moiré cell for the states shown in (a,b), plotted as functions of the number of remote-band pairs (n_{cut}) included in the projection-matrix formalism. Both quantities exhibit clear convergence for $n_{\text{cut}} \approx 20$. When evaluating M_{orb} , the chemical potential μ is fixed at the top of the valence band for $\nu = 3$ and at the bottom of the conduction band for $\nu = -3$, as indicated by the horizontal dashed lines in panels (a) and (b).

the other spin–valley flavors (shown in black), remain topological trivial. The symmetry breaking generates an indirect energy gap of approximately 13 meV between the occupied Chern band and the higher-energy bands. These states correspond to the experimentally observed quantum anomalous Hall phases with Chern number $C = 1$ ($C = -1$) at fillings $\nu = 3$ ($\nu = -3$) [2, 8, 45].

We next compute the orbital magnetization of these states using Eqs. 15 and 16. As shown in Fig.2(c,d), both the total orbital magnetization M_{orb} and the self-rotation component m_{SR} converge for $n_{\text{cut}} \approx 20$. Moreover, the results respect the particle–hole symmetry relating fillings $\nu = 3$ and $\nu = -3$, satisfying $M_{\text{orb}}(\nu = 3) = M_{\text{orb}}(\nu = -3)$, and $m_{\text{SR}}(\nu = 3) = -m_{\text{SR}}(\nu = -3)$ [69], consistent with the experimentally observed Landau fan structure[44, 45]. Since convergence is achieved for $n_{\text{cut}} \approx 20$, we adopt $n_{\text{cut}} = 30$ in the following calculations to ensure numerical stability.

One might be tempted to conclude that both the orbital magnetization M_{orb} and the self-rotation contribution m_{SR} arise exclusively from the occupied Chern bands that explicitly break time-reversal symmetry, and that only these bands need to be considered—analogous to the case of Berry curvature. Such reasoning, however, is not generally valid. Although the occupied states of the remote bands, $|u_n(\mathbf{k})\rangle$, remain invariant under time-reversal symmetry, their momentum derivatives $|\partial_{\mu} u_n(\mathbf{k})\rangle$ generally possess non-vanishing overlaps with those states in the active bands. Consequently, once time-reversal symmetry is broken within the active

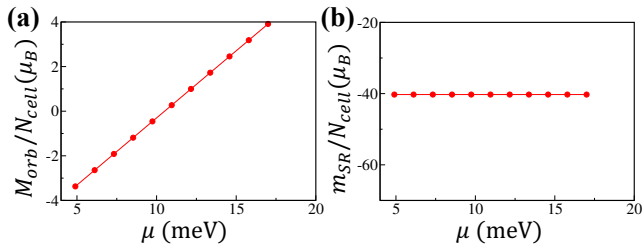


FIG. 3. Calculated total orbital magnetization M_{orb} (a) and self-rotation contribution m_{SR} (b) per moiré cell as functions of the chemical potential for the Chern insulating state at $\nu = 3$ inside the insulating gap, whose band dispersion is shown in Fig. 2(a). M_{orb} shows a linear dependence with μ and changes sign within the gap while m_{SR} remains constant. The number of remote band pairs n_{cut} is set to 30 in the calculation.

bands, the nominally time-reversal-symmetric remote bands acquire finite contributions to both M_{orb} and m_{SR} . The need to include a substantial number of remote bands—at least 20 pairs in our calculations—to achieve numerical convergence provides direct evidence of their non-negligible contributions.

More physically relevant is the behavior of M_{orb} and m_{SR} within the Chern insulating gap, indicated by the red dots in Fig. 3(a,b). The total orbital magnetization M_{orb} exhibits the expected linear dependence on μ . Thermodynamics gives the relation $\partial M_{\text{orb}}/\partial\mu = \partial N/\partial B$, consistent with the Diophantine equation that characterizes quantum Hall states. Taking the derivative of Eq. 11 with respect to μ yields

$$\frac{\partial M_{\text{orb}}}{\partial\mu} = S \frac{e}{h} C, \quad (19)$$

where C is the Chern number. The linear dependence leads to a sign reversal of M_{orb} across the gap, corresponding to magnetization reversal previously analyzed in the non-interacting case [55]. The in-gap plateau of m_{SR} demonstrates that the Chern insulating state possesses a large self-rotation contribution of approximately $40\mu_B$, which is directly accessible through magneto-optical probes such as magnetic circular dichroism.

B. Competing states at $\nu = \pm 1$

We next consider the correlated insulating states at fillings $\nu = \pm 1$. Owing to the particle-hole symmetry relating ν and $-\nu$, we focus on the case $\nu = 1$. The Hartree-Fock calculation yields two nearly degenerate correlated insulating states. The lowest-energy state is a mixed phase combining intervalley coherence (IVC) and $C_2\mathcal{T}$ symmetry breaking. In this state, the five valence bands consist of two bands associated with a spin-polarized IVC sector carrying zero Chern number, one $C_2\mathcal{T}$ -broken band with finite Chern number, and an additional pair of ungapped bands from one spin-valley flavor, resulting in a total Chern number $C = 1$ [22]. Its band dispersion is shown in Fig. 4(b). This state is lower in energy by approximately 0.5 meV per particle compared to the state in which

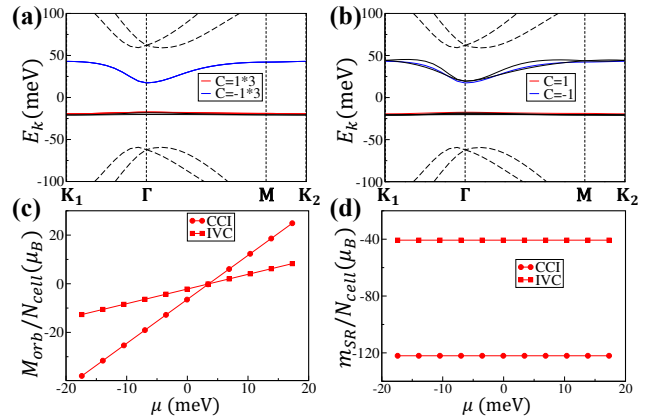


FIG. 4. (a,b) Band dispersions of the correlated Chern insulating state (CCI) (a) and the intervalley-coherent (IVC) state (b) at filling $\nu = 1$, obtained within the HF approximation. The solid curves represent the eight interaction-renormalized HF bands, while the dashed curves denote the remote bands excluded from the self-consistent HF calculation. Bands carrying nontrivial Chern numbers are highlighted in red ($C = 1$) and blue ($C = -1$). For the CCI, the Chern bands are triply degenerate, yielding a total Chern number $C = 3$. (c,d) Calculated total orbital magnetization M_{orb} (c) and self-rotation contribution m_{SR} (d) per moiré cell as functions of the chemical potential μ inside the insulating gap for the two states shown in (a) and (b). Solid circles correspond to the CCI, and solid squares to the IVC state. M_{orb} varies linearly with μ and changes sign across the gap, while m_{SR} remains constant. The number of remote band pairs n_{cut} is set to 30 in the calculation.

three valence bands break $C_2\mathcal{T}$ symmetry and each carries a finite Chern number. We refer to the latter as the correlated Chern insulator (CCI) with total Chern number $C = 3$, whose dispersion is shown in Fig. 4(a). We then compute the orbital magnetization for both states. As shown in Fig. 4(c), the total orbital magnetization M_{orb} for both states exhibits a linear dependence on the chemical potential within the insulating gap and changes sign across the gap. Both the magnitude and the slope of M_{orb} are larger for the CCI than for the mixed IVC state, reflecting its higher Chern number. This implies that the CCI is energetically favored in the presence of a finite magnetic field, consistent with experimental observations. Similarly, the self-rotation contribution m_{SR} of the CCI is significantly larger than that of the IVC state, as shown in Fig. 4(d).

V. CONCLUSION

In this work, we developed a practical and gauge-invariant framework to compute orbital magnetization in correlated states of magic-angle twisted bilayer graphene within self-consistent Hartree-Fock theory. Based on the projector formulation of the recently developed theory of orbital magnetization in the interacting system [56], we evaluated both the total orbital magnetization M_{orb} and the self-rotation contribution m_{SR} directly from the HF Hamiltonian and its eigenstates, thereby avoiding gauge ambiguities associated with Bloch-wavefunction derivatives. A key advantage of this approach

is that it enables controlled inclusion of remote-band effects through the projection matrices. We demonstrated that, unlike the Chern number, the orbital magnetization is highly sensitive to remote bands and requires careful convergence with respect to the number of remote band pairs n_{cut} , which saturates for $n_{\text{cut}} \gtrsim 20$ in our calculations.

Applying this method to integer fillings, we obtained converged orbital magnetization for the TRSB Chern insulating states at $\nu = \pm 3$ and for competing correlated phases at $\nu = 1$. Our results ensure the thermodynamic linear dependence of M_{orb} on the chemical potential inside the insulating gaps with the slope determined by the Chern number, while yielding a sizable and constant in-gap m_{SR} relevant for magneto-optical probes. More broadly, the gauge-invariant projector formalism introduced here provides a systematic route to quantify orbital magnetization in interaction-driven moiré phases and

can be readily extended to other moiré materials.

ACKNOWLEDGMENTS

We thank Hui-Ke Jin, Jie Wang, Minxuan Wang, Wen-Yu He, and especially Oskar Vafek for helpful discussions. J. K. acknowledges the support from the NSFC (Grant No. 12574159 and No. 12074276), the Double First-Class Initiative Fund of ShanghaiTech University, and the start-up grant of ShanghaiTech University. YZ is supported in part by the Shanghai Science and Technology Innovation Action Plan (Grant No. 24LZ1400800) and National Natural Science Foundation of China (NSFC) Grants No. 12274279. ZW is supported by the U.S. Department of Energy, Basic Energy Sciences, Grant No. DE FG02-99ER45747.

-
- [1] Yuan Cao, Valla Fatemi, Shiang Fang, Kenji Watanabe, Takashi Taniguchi, Efthimios Kaxiras, and Pablo Jarillo-Herrero, “Unconventional superconductivity in magic-angle graphene superlattices,” *Nature* **556**, 43–50 (2018).
- [2] Aaron L. Sharpe, Eli J. Fox, Arthur W. Barnard, Joe Finney, Kenji Watanabe, Takashi Taniguchi, M. A. Kastner, and David Goldhaber-Gordon, “Emergent ferromagnetism near three-quarters filling in twisted bilayer graphene,” *Science* **365**, 605–608 (2019).
- [3] Xiaobo Lu, Petr Stepanov, Wei Yang, Ming Xie, Mohammed Ali Aamir, Ipsita Das, Carles Urgell, Kenji Watanabe, Takashi Taniguchi, Guangyu Zhang, Adrian Bachtold, Allan H. MacDonald, and Dmitri K. Efetov, “Superconductors, orbital magnets and correlated states in magic-angle bilayer graphene,” *Nature* **574**, 653–657 (2019).
- [4] Yuhang Jiang, Xinyuan Lai, Kenji Watanabe, Takashi Taniguchi, Kristjan Haule, Jinhai Mao, and Eva Y. Andrei, “Charge order and broken rotational symmetry in magic-angle twisted bilayer graphene,” *Nature* **573**, 91–95 (2019).
- [5] Alexander Kerelsky, Leo J. McGilly, Dante M. Kennes, Lede Xian, Matthew Yankowitz, Shaowen Chen, K. Watanabe, T. Taniguchi, James Hone, Cory Dean, Angel Rubio, and Abhay N. Pasupathy, “Maximized electron interactions at the magic angle in twisted bilayer graphene,” *Nature* **572**, 95–100 (2019).
- [6] Yonglong Xie, Biao Lian, Berthold Jäck, Xiaomeng Liu, Cheng-Li Chiu, Kenji Watanabe, Takashi Taniguchi, B. Andrei Bernevig, and Ali Yazdani, “Spectroscopic signatures of many-body correlations in magic-angle twisted bilayer graphene,” *Nature* **572**, 101–105 (2019).
- [7] Youngjoon Choi, Jeannette Kemmer, Yang Peng, Alex Thomson, Harpreet Arora, Robert Polski, Yiran Zhang, Hechen Ren, Jason Alicea, Gil Refael, Felix von Oppen, Kenji Watanabe, Takashi Taniguchi, and Stevan Nadj-Perge, “Electronic correlations in twisted bilayer graphene near the magic angle,” *Nature Physics* **15**, 1174–1180 (2019).
- [8] M. Serlin, C. L. Tschirhart, H. Polshyn, Y. Zhang, J. Zhu, K. Watanabe, T. Taniguchi, L. Balents, and A. F. Young, “Intrinsic quantized anomalous hall effect in a moiré heterostructure,” *Science* **367**, 900–903 (2020).
- [9] Matthew Yankowitz, Shaowen Chen, Hryhorii Polshyn, Yuxuan Zhang, K. Watanabe, T. Taniguchi, David Graf, Andrea F. Young, and Cory R. Dean, “Tuning superconductivity in twisted bilayer graphene,” *Science* **363**, 1059–1064 (2019).
- [10] Yuan Cao, Valla Fatemi, Shiang Fang, Kenji Watanabe, Takashi Taniguchi, Efthimios Kaxiras, and Pablo Jarillo-Herrero, “Unconventional superconductivity in magic-angle graphene superlattices,” *Nature* **556**, 43–50 (2018).
- [11] Emilio Codecido, Qiyue Wang, Ryan Koester, Shi Che, Haidong Tian, Rui Lv, Son Tran, Kenji Watanabe, Takashi Taniguchi, Fan Zhang, Marc Bockrath, and Chun Ning Lau, “Correlated insulating and superconducting states in twisted bilayer graphene below the magic angle,” *Science Advances* **5**, eaaw9770 (2019).
- [12] Rafi Bistritzer and Allan H. MacDonald, “Moiré bands in twisted double-layer graphene,” *Proceedings of the National Academy of Sciences* **108**, 12233–12237 (2011).
- [13] Zhida Song, Zhijun Wang, Wujun Shi, Gang Li, Chen Fang, and B. Andrei Bernevig, “All magic angles in twisted bilayer graphene are topological,” *Phys. Rev. Lett.* **123**, 036401 (2019).
- [14] Zhi-Da Song, Biao Lian, Nicolas Regnault, and B. Andrei Bernevig, “Twisted bilayer graphene. ii. stable symmetry anomaly,” *Phys. Rev. B* **103**, 205412 (2021).
- [15] Junyeong Ahn, Sungjoon Park, and Bohm-Jung Yang, “Failure of nielsen-ninomiya theorem and fragile topology in two-dimensional systems with space-time inversion symmetry: Application to twisted bilayer graphene at magic angle,” *Phys. Rev. X* **9**, 021013 (2019).
- [16] Grigory Tarnopolsky, Alex Jura Kruchkov, and Ashvin Vishwanath, “Origin of magic angles in twisted bilayer graphene,” *Phys. Rev. Lett.* **122**, 106405 (2019).
- [17] Jianpeng Liu, Junwei Liu, and Xi Dai, “Pseudo landau level representation of twisted bilayer graphene: Band topology and implications on the correlated insulating phase,” *Phys. Rev. B* **99**, 155415 (2019).
- [18] Hoi Chun Po, Lijun Zou, T. Senthil, and Ashvin Vishwanath, “Faithful tight-binding models and fragile topology of magic-angle bilayer graphene,” *Phys. Rev. B* **99**, 195455 (2019).
- [19] Jian Kang and Oskar Vafek, “Strong coupling phases of partially filled twisted bilayer graphene narrow bands,” *Phys. Rev. Lett.* **122**, 246401 (2019).
- [20] Jian Kang and Oskar Vafek, “Non-abelian dirac node braiding and near-degeneracy of correlated phases at odd integer filling in magic-angle twisted bilayer graphene,” *Phys. Rev. B* **102**,

- 035161 (2020).
- [21] Ya-Hui Zhang, Dan Mao, and T. Senthil, “Twisted bilayer graphene aligned with hexagonal boron nitride: Anomalous hall effect and a lattice model,” *Phys. Rev. Res.* **1**, 033126 (2019).
- [22] Yi Zhang, Kun Jiang, Ziqiang Wang, and Fuchun Zhang, “Correlated insulating phases of twisted bilayer graphene at commensurate filling fractions: A hartree-fock study,” *Phys. Rev. B* **102**, 035136 (2020).
- [23] Xiao Yan Xu, K. T. Law, and Patrick A. Lee, “Kekulé valence bond order in an extended hubbard model on the honeycomb lattice with possible applications to twisted bilayer graphene,” *Phys. Rev. B* **98**, 121406 (2018).
- [24] Ming Xie and A. H. MacDonald, “Nature of the correlated insulator states in twisted bilayer graphene,” *Phys. Rev. Lett.* **124**, 097601 (2020).
- [25] Cheng-Cheng Liu, Li-Da Zhang, Wei-Qiang Chen, and Fan Yang, “Chiral spin density wave and $d + id$ superconductivity in the magic-angle-twisted bilayer graphene,” *Phys. Rev. Lett.* **121**, 217001 (2018).
- [26] Tongyun Huang, Lufeng Zhang, and Tianxing Ma, “Antiferromagnetically ordered mott insulator and $d+id$ superconductivity in twisted bilayer graphene: a quantum monte carlo study,” *Science Bulletin* **64**, 310–314 (2019).
- [27] Jianpeng Liu and Xi Dai, “Theories for the correlated insulating states and quantum anomalous hall effect phenomena in twisted bilayer graphene,” *Phys. Rev. B* **103**, 035427 (2021).
- [28] Shang Liu, Eslam Khalaf, Jong Yeon Lee, and Ashvin Vishwanath, “Nematic topological semimetal and insulator in magic-angle bilayer graphene at charge neutrality,” *Phys. Rev. Res.* **3**, 013033 (2021).
- [29] Nick Bultinck, Shubhayu Chatterjee, and Michael P. Zaletel, “Mechanism for anomalous hall ferromagnetism in twisted bilayer graphene,” *Phys. Rev. Lett.* **124**, 166601 (2020).
- [30] Nick Bultinck, Eslam Khalaf, Shang Liu, Shubhayu Chatterjee, Ashvin Vishwanath, and Michael P. Zaletel, “Ground state and hidden symmetry of magic-angle graphene at even integer filling,” *Phys. Rev. X* **10**, 031034 (2020).
- [31] Fengcheng Wu and Sankar Das Sarma, “Collective excitations of quantum anomalous hall ferromagnets in twisted bilayer graphene,” *Phys. Rev. Lett.* **124**, 046403 (2020).
- [32] Bin-Bin Chen, Yuan Da Liao, Ziyu Chen, Oskar Vafek, Jian Kang, Wei Li, and Zi Yang Meng, “Realization of topological mott insulator in a twisted bilayer graphene lattice model,” *Nature Communications* **12**, 5480 (2021).
- [33] Chen Lu, Yongyou Zhang, Yu Zhang, Ming Zhang, Cheng-Cheng Liu, Yu Wang, Zheng-Cheng Gu, Wei-Qiang Chen, and Fan Yang, “Chiral $so(4)$ spin-valley density wave and degenerate topological superconductivity in magic-angle twisted bilayer graphene,” *Phys. Rev. B* **106**, 024518 (2022).
- [34] Yuan Da Liao, Jian Kang, Clara N. Breiø, Xiao Yan Xu, Han-Qing Wu, Brian M. Andersen, Rafael M. Fernandes, and Zi Yang Meng, “Correlation-induced insulating topological phases at charge neutrality in twisted bilayer graphene,” *Phys. Rev. X* **11**, 011014 (2021).
- [35] B. Andrei Bernevig, Zhi-Da Song, Nicolas Regnault, and Biao Lian, “Twisted bilayer graphene. iii. interacting hamiltonian and exact symmetries,” *Phys. Rev. B* **103**, 205413 (2021).
- [36] Biao Lian, Zhi-Da Song, Nicolas Regnault, Dmitri K. Efetov, Ali Yazdani, and B. Andrei Bernevig, “Twisted bilayer graphene. iv. exact insulator ground states and phase diagram,” *Phys. Rev. B* **103**, 205414 (2021).
- [37] Fang Xie, Aditya Cowsik, Zhi-Da Song, Biao Lian, B. Andrei Bernevig, and Nicolas Regnault, “Twisted bilayer graphene. vi. an exact diagonalization study at nonzero integer filling,” *Phys. Rev. B* **103**, 205416 (2021).
- [38] Kasra Hejazi, Xiao Chen, and Leon Balents, “Hybrid wannier chern bands in magic angle twisted bilayer graphene and the quantized anomalous hall effect,” *Phys. Rev. Res.* **3**, 013242 (2021).
- [39] A. O. Sboychakov, A. V. Rozhkov, A. L. Rakhmanov, and Franco Nori, “Many-body effects in twisted bilayer graphene at low twist angles,” *Phys. Rev. B* **100**, 045111 (2019).
- [40] Louk Rademaker, Dmitry A. Abanin, and Paula Mellado, “Charge smoothening and band flattening due to hartree corrections in twisted bilayer graphene,” *Phys. Rev. B* **100**, 205114 (2019).
- [41] Francisco Guinea and Niels R. Walet, “Electrostatic effects, band distortions, and superconductivity in twisted graphene bilayers,” *Proceedings of the National Academy of Sciences* **115**, 13174–13179 (2018).
- [42] Kangjun Seo, Valeri N. Kotov, and Bruno Uchoa, “Ferromagnetic mott state in twisted graphene bilayers at the magic angle,” *Phys. Rev. Lett.* **122**, 246402 (2019).
- [43] Shuang Wu, Zhenyuan Zhang, K. Watanabe, T. Taniguchi, and Eva Y. Andrei, “Chern insulators, van hove singularities and topological flat bands in magic-angle twisted bilayer graphene,” *Nature Materials* **20**, 488–494 (2021).
- [44] Ipsita Das, Xiaobo Lu, Jonah Herzog-Arbeitman, Zhi-Da Song, Kenji Watanabe, Takashi Taniguchi, B. Andrei Bernevig, and Dmitri K. Efetov, “Symmetry-broken chern insulators and rashba-like landau-level crossings in magic-angle bilayer graphene,” *Nature Physics* **17**, 710–714 (2021).
- [45] Kevin P. Nuckolls, Myungchul Oh, Dillon Wong, Biao Lian, Kenji Watanabe, Takashi Taniguchi, B. Andrei Bernevig, and Ali Yazdani, “Strongly correlated chern insulators in magic-angle twisted bilayer graphene,” *Nature* **588**, 610–615 (2020).
- [46] Petr Stepanov, Ming Xie, Takashi Taniguchi, Kenji Watanabe, Xiaobo Lu, Allan H. MacDonald, B. Andrei Bernevig, and Dmitri K. Efetov, “Competing zero-field chern insulators in superconducting twisted bilayer graphene,” *Phys. Rev. Lett.* **127**, 197701 (2021).
- [47] Jiachen Yu, Benjamin A. Foutty, Zhaoyu Han, Mark E. Barber, Yoni Schattner, Kenji Watanabe, Takashi Taniguchi, Philip Phillips, Zhi-Xun Shen, Steven A. Kivelson, and Benjamin E. Feldman, “Correlated hofstadter spectrum and flavour phase diagram in magic-angle twisted bilayer graphene,” *Nature Physics* **18**, 825–831 (2022).
- [48] Wen-Yu He, David Goldhaber-Gordon, and K. T. Law, “Giant orbital magnetoelectric effect and current-induced magnetization switching in twisted bilayer graphene,” *Nature Communications* **11**, 1650 (2020).
- [49] Ying Su and Shi-Zeng Lin, “Current-induced reversal of anomalous hall conductance in twisted bilayer graphene,” *Phys. Rev. Lett.* **125**, 226401 (2020).
- [50] Chunli Huang, Nemin Wei, and Allan H. MacDonald, “Current-driven magnetization reversal in orbital chern insulators,” *Phys. Rev. Lett.* **126**, 056801 (2021).
- [51] Jong Yeon Lee, Eslam Khalaf, Shang Liu, Xiaomeng Liu, Zeyu Hao, Philip Kim, and Ashvin Vishwanath, “Theory of correlated insulating behaviour and spin-triplet superconductivity in twisted double bilayer graphene,” *Nature Communications* **10**, 5333 (2019).
- [52] Shihao Zhang, Xi Dai, and Jianpeng Liu, “Spin-polarized nematic order, quantum valley hall states, and field-tunable topological transitions in twisted multilayer graphene systems,” *Phys. Rev. Lett.* **128**, 026403 (2022).

- [53] Jianpeng Liu, Zhen Ma, Jinhua Gao, and Xi Dai, “Quantum valley hall effect, orbital magnetism, and anomalous hall effect in twisted multilayer graphene systems,” *Phys. Rev. X* **9**, 031021 (2019).
- [54] Jianpeng Liu and Xi Dai, “Orbital magnetic states in moirégraphene systems,” *Nature Reviews Physics* **3**, 367–382 (2021).
- [55] Jihang Zhu, Jung-Jung Su, and A. H. MacDonald, “Voltage-controlled magnetic reversal in orbital chern insulators,” *Phys. Rev. Lett.* **125**, 227702 (2020).
- [56] Jian Kang, Minxuan Wang, and Oskar Vafek, “Orbital magnetization and magnetic susceptibility of interacting electrons,” *arXiv e-prints*, arXiv:2509.20626 (2025).
- [57] Jihang Zhu and Chunli Huang, “Magnetic-Field-Induced Geometric Response of Mean-Field Projectors: Streda Formula and Orbital Magnetization,” *arXiv e-prints*, arXiv:2510.07001 (2025).
- [58] Xiaoyu Liu, Chong Wang, Xiao-Wei Zhang, Ting Cao, and Di Xiao, “Orbital Magnetization in Correlated States of Twisted Bilayer Transition Metal Dichalcogenides,” *arXiv e-prints*, arXiv:2510.01727 (2025).
- [59] Mengxing Ye, “A Quantum Many-Body Approach for Orbital Magnetism in Correlated Multiband Electron Systems,” *arXiv e-prints*, arXiv:2601.14372 (2026).
- [60] Xi Chen and Zhi-Da Song, “Orbital Magnetization of Interacting Electrons,” *arXiv e-prints*, arXiv:2602.02478 (2026).
- [61] Davide Ceresoli, T. Thonhauser, David Vanderbilt, and R. Resta, “Orbital magnetization in crystalline solids: Multi-band insulators, chern insulators, and metals,” *Phys. Rev. B* **74**, 024408 (2006).
- [62] J. M. B. Lopes dos Santos, N. M. R. Peres, and A. H. Castro Neto, “Continuum model of the twisted graphene bilayer,” *Phys. Rev. B* **86**, 155449 (2012).
- [63] Hoi Chun Po, Liujun Zou, Ashvin Vishwanath, and T. Senthil, “Origin of mott insulating behavior and superconductivity in twisted bilayer graphene,” *Phys. Rev. X* **8**, 031089 (2018).
- [64] Hoi Chun Po, Haruki Watanabe, and Ashvin Vishwanath, “Fragile topology and wannier obstructions,” *Phys. Rev. Lett.* **121**, 126402 (2018).
- [65] Jian Kang, B. Andrei Bernevig, and Oskar Vafek, “Cascades between light and heavy fermions in the normal state of magic-angle twisted bilayer graphene,” *Phys. Rev. Lett.* **127**, 266402 (2021).
- [66] Ivo Souza and David Vanderbilt, “Dichroic f -sum rule and the orbital magnetization of crystals,” *Phys. Rev. B* **77**, 054438 (2008).
- [67] Raffaele Resta, “Magnetic circular dichroism versus orbital magnetization,” *Phys. Rev. Res.* **2**, 023139 (2020).
- [68] Guangyue Ji, David E. Palomino, Nathan Goldman, Tomoki Ozawa, Peter Riseborough, Jie Wang, and Bruno Mera, “Density Matrix Geometry and Sum Rules,” *arXiv e-prints*, arXiv:2507.14028 (2025).
- [69] See Supplemental Material for more detailed discussions.